Inter-decadal changes of thermodynamic stability variables in a transatlantic section along 7.5º N.

Miguel Ángel San Antolín Plaza

Supervisors: Josep Lluís Pelegrí [2] and Francisco José Machín [1].

[1] Facultad de Ciencias del Mar, Universidad de Las Palmas G. C., Campus de Tafira, 35017 Las Palmas, Spain .
[2] Institut de Ciències del Mar, CSIC, Passeig Marítim de la Barceloneta 37-49, 08003 Barcelona, Spain.

Abstract

We analyse inter-decadal variations, between 1957 and 2010, of different thermodynamic stability variables in a transatlantic section along 7.5ºN. The results reveal an enhancement of small-scale activity between 1993 and 2010, with the mean number of density overturns per station increasing from 250 ± 70 to 390 ± 70, but retaining similar mean vertical extension (about 2 ± 0.4 m). The integrated buoyancy frequency experienced an important relative increase from 1957 to 2010: up to 15% for central waters, 8% for intermediate waters or 2% for upper-deep waters, if the water column is divided in depth ranges. When using neutral density ranges, a 20% increase occurs for central and intermediate waters, but error intervals increase. The Turner angle distributions highlight a predominance of salt-fingering, related to the unstable salinity distribution in the North Atlantic, whereas diffusive convection appears sparsely. A gravitationally stable layer is present between approximately 800 m and 1500 - 2000 m depth (widening eastwards) below the intermediate waters core. The lower limit of this layer was shallowest in 2010, due to the mayor appearance of the salty Upper North Atlantic Deep Water (UNADW); this zone changing from gravitationally stable to salt fingering regime. The thermodynamic stability is studied by examining the displacements in αθ-βS diagrams (being α and β the thermal expansion and haline contraction coefficients, θ the potential temperature and S the salinity). Surface, central and upper-intermediate waters appear in this plane nearly as a constant βS value, whereas deep waters show up nearly as an αθ isoline. The relatively fresher intermediate waters and salty upper-deep waters show a transition zone. Thermodynamic displacements show relatively small changes, always less than 0.5%.

1. Introduction.

The WOCE A06 transect has been carried out three times from 1957 to 2010. The two early realizations were done first in 1957 along 8.25ºN as part of the International Geophysical Year (Fuglister, 1960) and later along 7.5ºN in 1993 within the World Ocean Circulation Experiment (Arhan et al., 1998). In April-May 2010 the BIO Hespérides carried out a new transatlantic section along 7.5ºN. A fourth transatlantic cruise in the equatorial North Atlantic took place in July 2000 by Lappo et al. (2001), but following substantially different track, therefore it is not considered in this analysis.

Although the paths and spatial resolutions for each realization slightly differ from each other, the available data set allows us to make an inter-decadal comparison of the ocean structure. This work focuses on the changes in stability, mixing processes and thermodynamic displacements between all three realizations. The study is carried out with the aid of the following derived variables: Brunt-Väisälä frequency, Turner angle, and a novel variable measuring the contribution of thermodynamic displacements to density changes. Also the distributions of these variables are presented. The methodology here introduced may be extended to other transoceanic transects, with the purpose of obtaining a deeper understanding of these variables and their inter-decadal variability.

The potential importance of double-diffusive processes to large-scale remains an open question (Ruddick, 2003). Furthermore, the presence of the turbulence might inhibit the formation of double-diffusive structures, even when temperature and salinity gradients are favourable (You et al, 2003). The choice of proper vertical resolutions is therefore fundamental for the correct study of each variable and phenomenon. All the information referent to the data set and interpolation, filtering and general methodology of the work is introduced in chapters two and three. In chapters four, five and six static stability, double – diffusive processes and the thermodynamic displacement are respectively analysed. Finally, the most relevant conclusions are summarised in the seventh chapter.

2. Data set

The hydrographic data for the WOCE A06 transect have been obtained during three cruises carried out in 1957, 1993 and 2010. Data longitudinal resolution, related to the number and location of the stations, presents similar order for all transects. However, the vertical resolution of the 1957 data is much lower, as this set of data was obtained with bottle water samples. The different spatial resolutions of the three data sets make necessary the construction of a data mesh with equivalent resolution, which enables the comparison and hence the study of the inter-decadal variability of the variables of interest. A detailed analysis of the 1957 and 1993 cruises has been reported elsewhere (Fuglister, 1957; Arhan et al., 1998; Oudot et al., 1998; Marin and Gouriou, 2000; Lux et al., 2001).

During the 2010 cruise the hydrographic stations had a spatial resolution of half a degree in the western Atlantic, until the Mid-Atlantic Ridge (MAR), and about one degree in the eastern margin. The hydrographic stations included a conductivity-temperature-depth (CTD) probe that sampled the water column down to the sea bottom with a 1-m vertical resolution. The location of the stations is shown in Figure 1. Due to the different paths followed in each campaign, the zonal interval useful for comparison extends between 47.5ºW and 15ºW. Boundary systems, in which an intense activity of currents and diapycnal processes take place, are therefore excluded from our region of study.

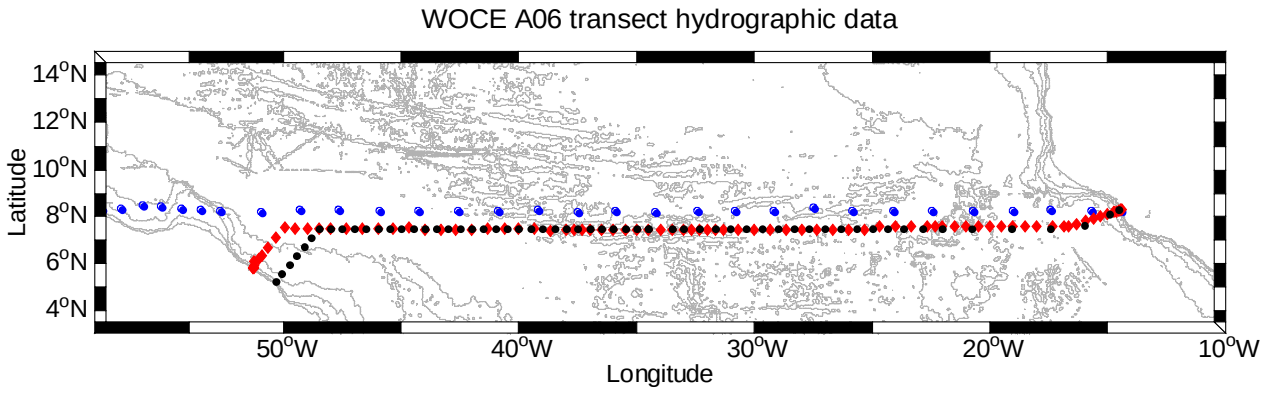

Figure 1. WOCE A06 transect for the 1957 (blue circles), 1993 (red diamonds) and 2010 (black dots) cruises.

3. Methods

Gravitational instabilities manifest as inversions (overturns) in the potential density profile and their scale can be determined using the Thorpe scale (Thorpe, 1977). According to this criterion, the number of overturns and their vertical extension will be determined for the 1993 and 2010 cruises since their original vertical data resolution of 1 m enables the proper study of these structures. A common longitudinal grid at 7.5ºN between 47.5ºW and 15ºW (with 1m vertical resolution) has been developed to enable the inter-decadal comparison of the potential density overturns. The study of the instability scales is carried out using the raw CTD data, interpolated in pressure and longitude in order to obtain a common grid that enables the comparison between both repetitions.

After the analysis of these overturns, the vertical resolution adopted for the rest of the study is 10 m. Temperature and salinity fields of 1993 and 2010 are also vertically smoothed using a low-pass Butterworth filter (of 0.4 normalised frequency threshold). This filtering removes small-scale overturns (of the order of several meters) preserving the information of the signal. The derived variables are calculated in the same manner from the new filtered temperature and salinity fields of 10 m vertical resolution. 1957 data do not need a filtering process since they have been already smoothed during the interpolation due to their sparse original vertical resolution.

Static stability may be described with the aid of the buoyancy or Brunt-Väisälä frequency, defined as

$$N = \left(-\frac{g}{\rho_\theta} \frac{\partial \rho_\theta}{\partial dz} \right)^{1/2} \quad (1)$$

where g is the gravity acceleration at every point, ρ_θ is the potential density calculated using a potential temperature θ referenced to the sea surface, and z is depth. Positive values of this frequency involve stable stratification, whereas negative ones values correspond to divergent displacements joined to unstable stratification.

Despite of the mentioned temperature and salinity filtering, some negative values of the buoyancy frequency still remain. These values are recalculated using an algorithm that removes density overturns of every scale using the Thorpe analysis as follows: when the beginning of an overturn is found, its Thorpe scale is calculated and the density profile smoothed, recalculating the buoyancy frequency values in between. This process might nevertheless generate artifacts, so buoyancy frequency must be smoothed at the end of the process. This second filtering is carried out with the aid of another low pass Butterworth filter (0.1) that deletes the mentioned artifacts and at the same time smooths the contours of the high – variablility bouyancy frequency signal. In fact, changes in the integrated values of the variables due to filtering are neglectable, so that its principal advantage consist in reducing the intervals of statistic errors and improving the visualization of the contours.

Turner angle is chosen (Ruddick, 1983) to analyze the stability of a water parcel to changes in its buoyancy associated to double-diffusive mixing processes. The Turner angle is defined as

$$Tu = \tan^{-1}\left(\frac{\alpha\Delta\theta - \beta\Delta S}{\alpha\Delta\theta + \beta\Delta S}\right) \tag{2}$$

where $\alpha = -\rho^{-1}\partial_\theta\rho$ is the thermal expansion coefficient and $\beta = \rho^{-1}\partial_S\rho$ is the haline contraction coefficient of seawater. The Turner angle characterizes several regimes with different stability conditions. For -45º < *Tu* < 45º the water column is stable in terms of $\partial_z\theta$ (positive gradient) and $\partial_z S$ (negative gradient), the salt-finger regime prevails for 45º < *Tu* < 90º while the diffusive regime occurs for -90º < *Tu* < -45º. Furthermore, |Tu| > 90º involves gravitational instabilities.

One chapter of this study will be dedicated to quantify the thermodynamic displacements experimented by the different points of the interpolated grid. Water masses are commonly described through θ-S diagrams. Our aim here is nevertheless to accomplish a dimensionless description in which salinity and potential temperature variations are directly comparable; in this case trough their effect on potential density variations. This is accomplished with the help of the coefficients α and β,

so that the effect of salinity and potential temperature changes in the potential density is given by $d\rho_\theta/\rho_\theta = -\alpha d\theta + \beta dS$. Therefore, we may define a variable representing a thermodynamic infinitesimal displacement in the αθ-βS plane as follows:

$$dl^2 = d(\alpha\theta)^2 + d(\beta S)^2 \tag{3a}$$

If we wish to calculate finite-distance displacements between data points from two different stations, e.g. from data points at different positions during the same cruise or from data points at the same position for two different cruises, the above expression should be integrated between the initial and final states in the αθ-βS space. The result is given by the following expression:

$$l^2 = (\alpha_f \cdot \theta_f - \alpha_i \cdot \theta_i)^2 + (\beta_f \cdot S_f - \beta_i \cdot S_i)^2 \tag{3b}$$

where the subscripts f and i indicate the final and initial state.

4. Vertical overturns and buoyancy frequency.

The analysis of the potential density profiles for the 1993 and 2010 interpolated data between 47.5ºW and 15ºW (56 interpolated stations of 1m vertical resolution) reveals a large amount of vertical density overturns along the water column. The methodology used here does not pay attention to the scale of the overturns, simply counting and determining the vertical extension of every overturn found, so that small overturns may be contained in a larger one.

The majority of the overturns that have been observed are of small scale, with a typical extension of a few meters (< 15 m). When analysing the water column for both realizations, the mean number of overturns per profile and the mean vertical extension per overturn show considerable differences: 500 ± 200 overturns per profile with a mean vertical extension of 7 ± 2 m for 1993 as compared with 700 ± 200 overturns per profile with a mean vertical extension of 3.7 ± 0.5 m for 2010. The

observed difference may be caused by the seasonal variability of the surface waters (shallower than 150 m) since both cruises show a lag of around two months. Indeed, once the shallowest waters (up to 150 m) are removed, the number of overturns per profile remain almost invariable (few overturns in the surface waters), but the mean vertical extension is drastically shortened (mainly as a result of removing the large overturns in the surface region), reaching 2.0 ± 0.4 m in 1993 and 1.8 ± 0.3 m for 2010. This fact confirms that the main cause of the original differences in the mean vertical extension per overturn was the seasonal variability of surface waters. On the other hand, we must consider before continuing that deep-water overturns are mostly related to the highly non-linear character of the equation of state. Potential density is calculated referenced to a very-far sea-surface pressure, giving rise to the appearance of these deep-water apparent overturns. In fact, when waters below 3000m are studied using a potential density referred to 3000 m, bottom overturns are drastically reduced (shorter than 100 m when values referenced to sea surface reached more than 1000 m). For this reason, in this work we ignore hereafter all the overturns deeper than 3000 m. With this consideration, results present important changes. Of course, the mean number of overturns per profile decreases, reaching the values 250 ± 70 for 1993 and 390 ± 70 for 2010, and the mean vertical extension falls down, to 1.5 ± 0.2 and 1.38 ± 0.09 for 1993 and 2010 respectively.

The number of overturns per profile (even when normalized by the mean depth of the stations) remains considerably larger for the 2010 cruise, what might be indicative of more intense sub-mesoscale mixing processes. For both realizations the longitudinal distribution of the number of overturns per profile (once normalized by depth) presents a slight asymmetry, with values below the mean eastward 28ºW for 1993 and 29ºW for 2010, and above the mean for the western half. This distribution may reflect the existence of different mixing processes in the eastern and western basins of the equatorial Atlantic, approximately separated by the MAR.

The study of the squared buoyancy frequency distributions shown in Figure 2 reveals four features

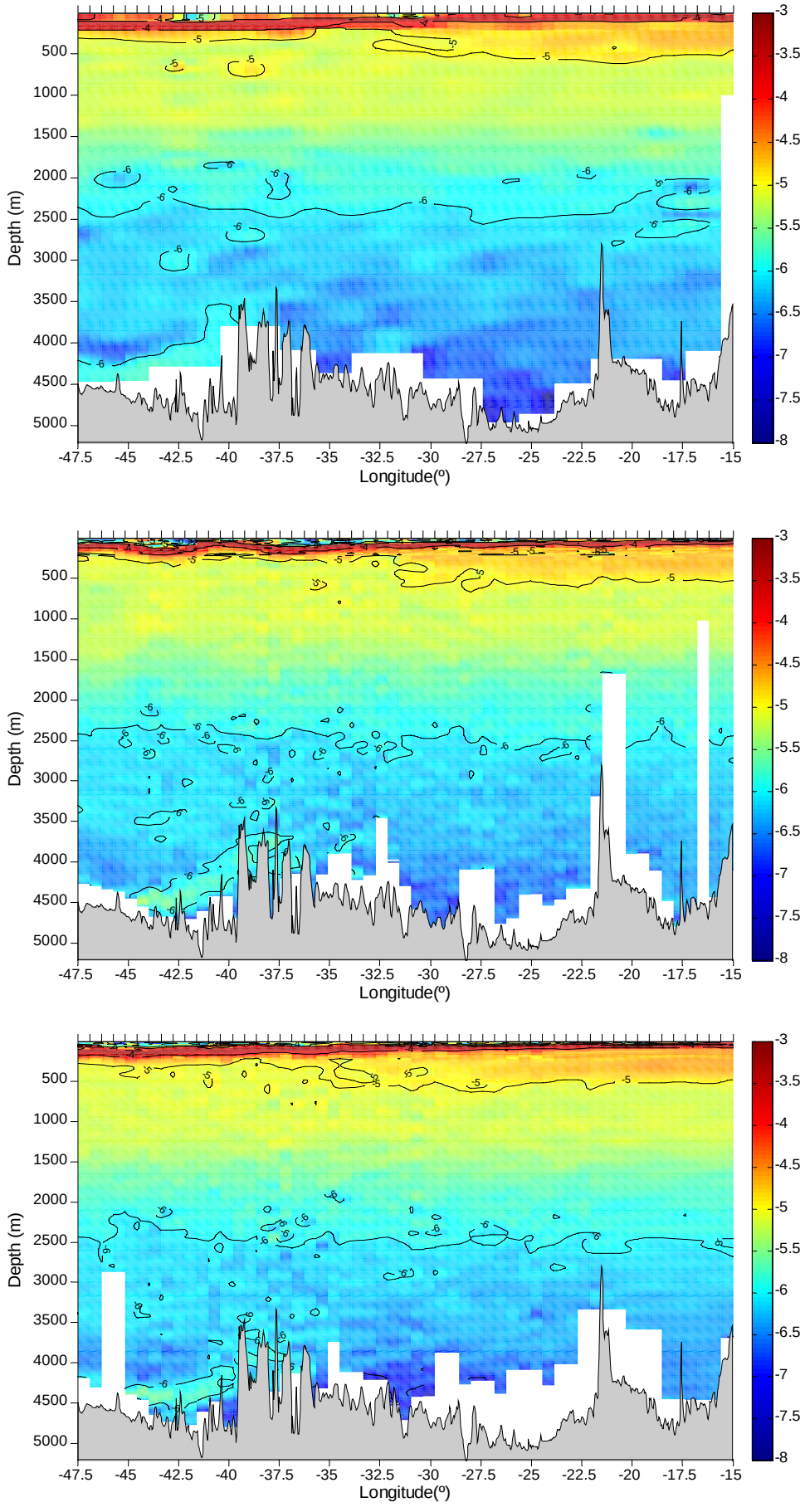

Figure 2. Squared buoyancy frequency distributions (s^{-2}) for 1957, 1993 and 2010 cruises (upper, mid and lower panels)

that should be mentioned. Firstly, the shallowest waters (mixing layer) show very low stability due to the high homogeneity of their properties and the active mixing present. Excepting this surface mixed layer, the static stability decreases with depth, with maximum values in the upper permanent thermocline (approximately in the 50-200 m range). Another important feature is the zonal asymmetry of central waters, with stability considerably higher in the eastern half of the basin, suggesting different water masses composition for each margin. Finally, the appearance of Antarctic Bottom Water (AABW) at the lower left corner is detectable through slightly higher frequency values. The differences between these three distributions will be carefully studied when analyzing the inter-decadal buoyancy frequency variability.

With the aim of comparing the three distributions, the averaged values of the squared buoyancy frequency are indicated in Table 1. The method is based on averaging the frequency value for every depth layer and afterwards obtaining a mean value for each depth interval. Results show very small changes in the average values but a significant increase for bottom waters.

	CW	IW	UDW	MDW	LDW	BW
1957	$(1.3 \pm 0.3) \times 10^{-5}$	$(7.2 \pm 0.6) \times 10^{-6}$	$(5 \pm 2) \times 10^{-6}$	$(1.0 \pm 0.5) \times 10^{-6}$	$(5.4 \pm 0.5) \times 10^{-7}$	$(3 \pm 2) \times 10^{-7}$
1993	$(1.2 \pm 0.3) \times 10^{-5}$	$(7.2 \pm 0.6) \times 10^{-6}$	$(5 \pm 2) \times 10^{-6}$	$(1.2 \pm 0.5) \times 10^{-6}$	$(6.5 \pm 0.4) \times 10^{-7}$	$(5 \pm 2) \times 10^{-7}$
2010	$(1.4 \pm 0.3) \times 10^{-5}$	$(7.5 \pm 0.6) \times 10^{-6}$	$(5 \pm 2) \times 10^{-6}$	$(1.1 \pm 0.5) \times 10^{-6}$	$(5.7 \pm 0.7) \times 10^{-7}$	$(6 \pm 2) \times 10^{-7}$

Table 1. Integrated values of squared buoyancy frequency for the different regions of the water column. CW: central waters (200 – 500m); IW: intermediate waters (500 – 1100 m); UDW: upper deep waters (1100 – 1700 m); MDW: mid deep waters (1700-3400 m); LDW: lower deep waters (3400-4000 m); BW: bottom waters (> 4000 m).

Figure 3 contains the buoyancy frequency anomaly distribution for 2010. The water column appears divided into four different regions (following Ahran *et al.*, 1998): surface waters (up to 200 m), central waters (200-500 m range) and intermediate waters (500-1100 m), while depth and bottom waters are contained in the same interval (1100 m-bottom). This division makes possible to plot four different regions that, in spite of their continuity along the water column, represent different buoyancy frequency and anomaly scales. Within the top 1000 m, the buoyancy frequency anomaly

distribution shows several zonal tongues extending along the whole section. These tilted layers raise eastwards conforming apparent continuous structures. In the upper thermocline, the anomaly has a dominant sign within one half of the section and the opposite one within the other half. However, whereas positive anomalies are observed in the western half for surface waters, the positive anomaly in the eastern margin is found for central waters (Figure 3). Positive anomalies are again observed in the western half for intermediate waters and even deep waters, though for intermediate waters the distribution begins to show patchiness, which becomes even more intense for deep waters. We may therefore affirm that the zonal structure of the ocean depends on the depth range and the different water masses composition of the different margins.

The reference mean profile for the 2010 interpolated data is plotted in Figure 4 on top all data points. With the aid of this diagram a correspondence between depth and potential density ranges can be estimated. The zonal average values of potential density for the depth interfaces separating different water regions shows values slightly smaller than those inferred from Figure 4, what suggests that the depth interfaces chosen, though consistent with literature could be shallower than observed. Anyway, these isolines must be taken as a reference value, since the zonal water masses

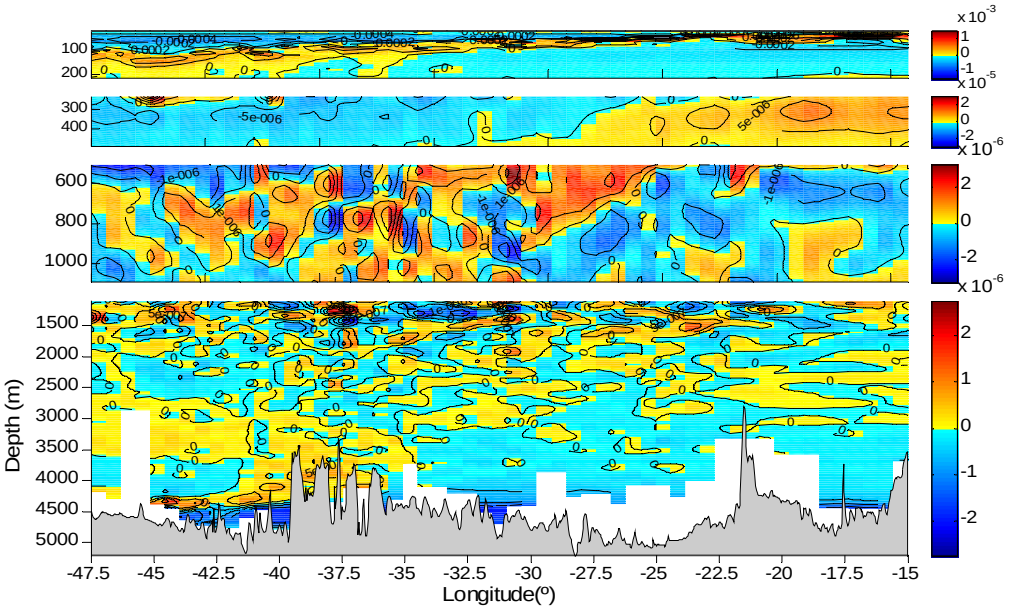

Figure 3. Distribution of squared buoyancy frequency anomaly (s^{-2}); 2010 transect. Note the different order of the colour scales for the different regions.

composition of the equatorial Atlantic shows an evident inhomogeneity, as can be inferred from the gap (under the red curve) within the central waters curve, which appears between two distinct central water masses, namely, the North Atlantic Central Water (NACW) and the South Atlantic Central Water (SACW).

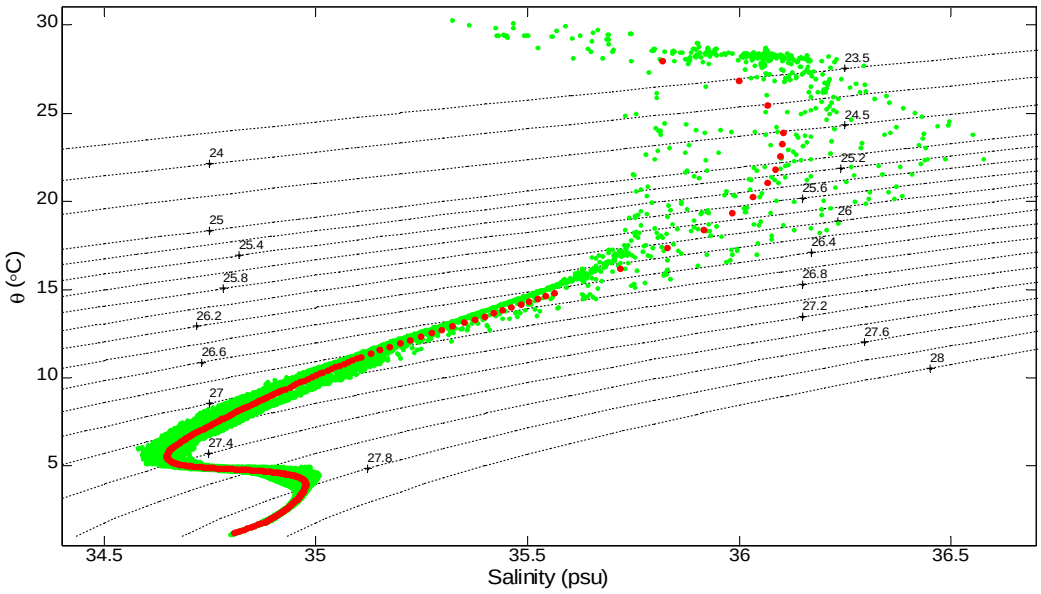

Figure 4. θ-S diagram 2010 transect. The original data interpolated in depth are plotted in green, whereas the red curve shows the reference profile calculated as a zonal mean for the different depth layers.

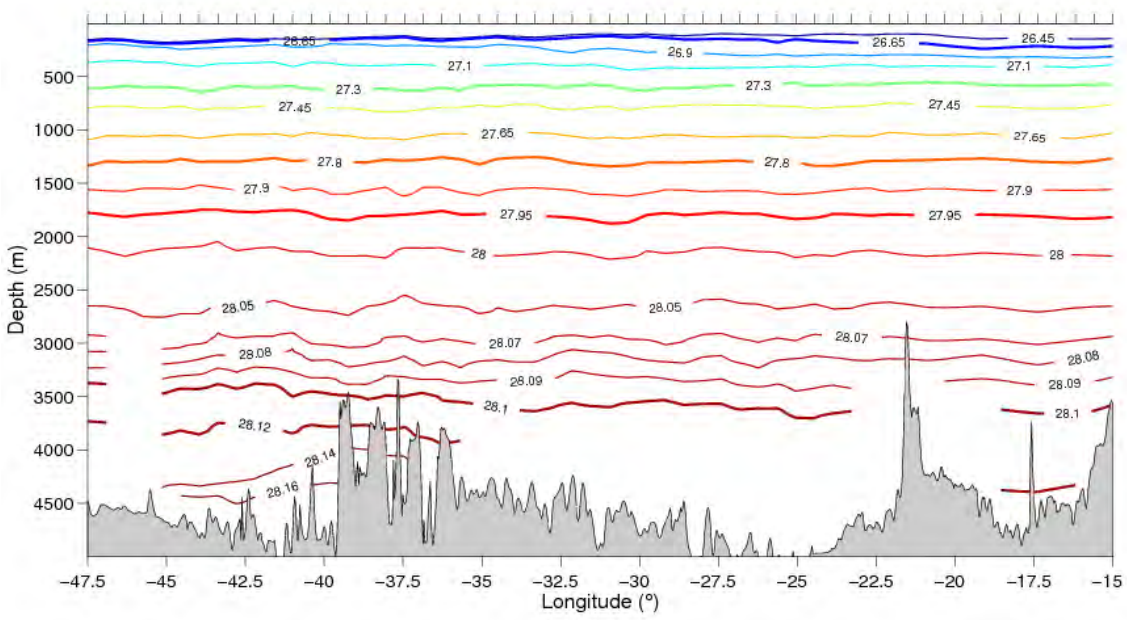

Figure 5. Neutral density contours for 2010 interpolated data. Contours separating water column regions (γ^n = 26.65, 27.3, 27.8 and 28.12) as well as the interfaces upper/ mid and mid/lower deep waters at (γ^n = 27.95, 28.1) are shown.

For the case of neutral density and as approximation for the whole basin (for better accuracy the basin should be regionally divided), surface waters would be present for $\gamma^n < 26.65$, central waters within the range $26.65 < \gamma^n < 27.3$, intermediate for $27.3 < \gamma^n < 27.8$, deep waters are confined to $27.8 < \gamma^n < 28.12$ and bottom waters appear for $\gamma^n > 28.12$ (Figure 5). These intervals show differences with the potential density ranges. For instance, the isopycnals separating surface and central waters, central and intermediate waters, the intermediate/deep waters interface and the boundary between deep and bottom layers are located at σ_θ = 26.65, 27.2 (intermediate waters occupy the range S < 34.7), 27.6 (the maximum in salinity below 5ºC identifies the core of UNADW) and 27.88 respectively (Figure 4).

Once the water column regions have been defined, the distribution of the buoyancy frequency and its anomaly can be represented using isoneutral coordinates. Figure 6 contains the buoyancy frequency distribution in this representation for the 2010 set of data. The map appears divided in water regions according to the defined neutral density ranges. It is noticeable that the buoyancy frequency range of values obtained using neutral density coordinates are smaller than using depth, as density overturns are eluded in this representation.

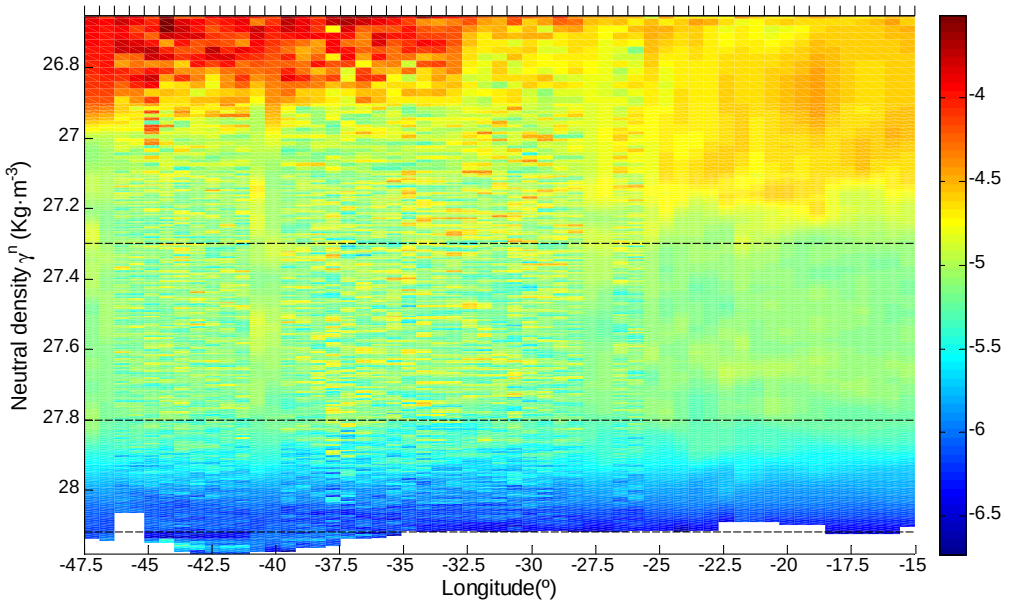

Figure 6. Squared buoyancy frequency (s^{-2}) distribution for 2010 interpolated data. The horizontal lines show the mean interfaces respectively separating central, intermediate, deep and bottom waters. Surface waters are not included.

As already observed in Figure 2 (lower panel), the zonal inhomogeneity of central waters suggests different values for the interface for every half of the basin since the eastern and the western margin differ in their water masses composition and stability ranges. Underneath these waters, the buoyancy frequency exhibits a zonal homogeneity and values depends mostly on neutral density (except for AABW appearing on the left lower corner, which shows values of buoyancy frequency larger than those of their immediately superior waters).

The averaged values for the different water column regions, defined according to neutral density ranges, are estimated in Table 2. As the definition of the water column regions for both coordinates do not exactly coincide, and both representations relate to different changes, differences with values in Table 1 exist. However, the average values show high similarity with those in Table 1, except for central waters (indirectly in contact with the atmosphere trough the mixed surface layers) and bottom waters (affected by bottom topography). The neutral density representation accurately shows the appearance of Antarctic Bottom Water (AABW) in the western margin.

	CW	**IW**	**UDW**	**MDW**	**LDW**	**BW**
1957	$(2 \pm 2) \times 10^{-5}$	$(7.1 \pm 0.7) \times 10^{-6}$	$(4 \pm 2) \times 10^{-6}$	$(1.1 \pm 0.5) \times 10^{-6}$	$(5.5 \pm 0.5) \times 10^{-7}$	$(1.2 \pm 0.4) \times 10^{-6}$
1993	$(2 \pm 2) \times 10^{-5}$	$(8 \pm 1) \times 10^{-6}$	$(4 \pm 2) \times 10^{-6}$	$(1.2 \pm 0.5) \times 10^{-6}$	$(6.0 \pm 0.5) \times 10^{-7}$	$(1.6 \pm 0.7) \times 10^{-6}$
2010	$(1.7 \pm 0.9) \times 10^{-5}$	$(8 \pm 1) \times 10^{-6}$	$(4 \pm 2) \times 10^{-6}$	$(1.2 \pm 0.4) \times 10^{-6}$	$(6.0 \pm 0.6) \times 10^{-7}$	$(1.3 \pm 0.5) \times 10^{-6}$

Table 2. Integrated values of squared buoyancy frequency (s^{-2}) for the different regions using neutral density ranges. CW: (26.7-27.3); IW: (27.3-27.8); UDW: (27.8 -27.95); MDW: (27.95 -28.1); LDW: (28.1 -28.12); BW: (>28.12).

Once the buoyancy frequency distributions have been described, we turn next to examine inter-decadal changes in the buoyancy frequency distribution. For this purpose we choose the relative variability of the squared buoyancy frequency, defined as $[(n^2_f - n^2_i)/ |n^2_i|]$, where *f* and *i* denote the final and initial state. Figure 7 shows the maps for the squared buoyancy frequency temporal variability. Intense patchiness is the most obvious feature of these maps. The upper panel illustrates the relative change between 1957 an 1993. A striking feature of this distribution is a large relative diminution of the buoyancy frequency immediately above the bottom and close to the zonal

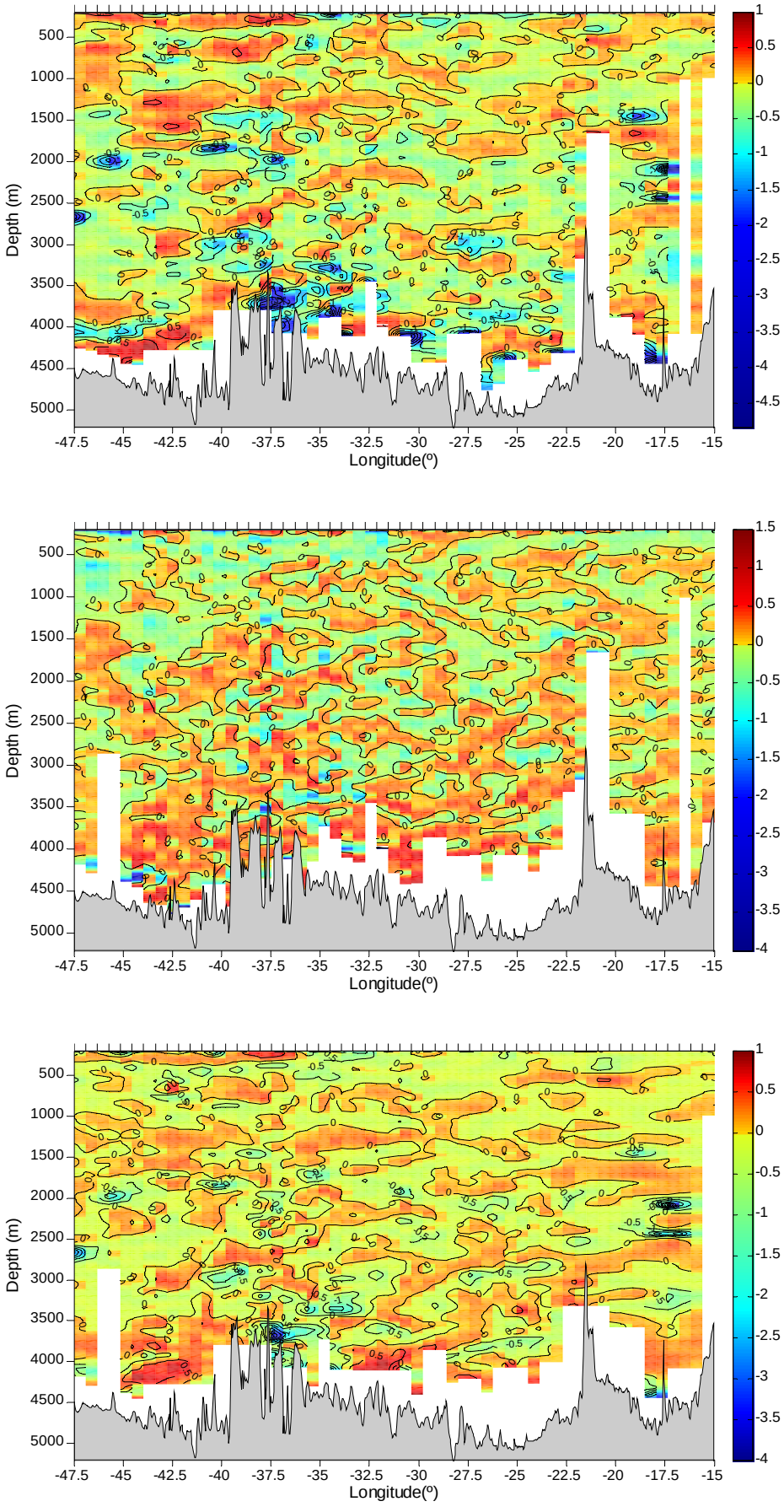

Figure 7. Squared buoyancy frequency relative variation. Positive values indicate increase and negative ones decrease. Upper, mid and lower panels respectively represent 1957-1993, 1993-2010 and 1957-2010 variations.

boundaries, probably related to either the presence of density overturns leading to a strong reduction of the buoyancy frequency values or the presence of mesoscale structures.

The relative variability between 1993 an 2010 (middle panel of Figure 7) reveals the predominance of increasing buoyancy frequency along the whole section. Central waters exhibits nevertheless a frequency diminution practically for every longitude. Negative patches have seemingly disappeared. Finally, the bottom panel in Figure 7 illustrates the trend for the whole 1957 to 2010 period. The map reveals a high similarity with the upper panel. This suggests that changes between 1957 and 1993 have been dominant over those between 1993 and 2010, albeit the smoother character of the 1957 data may play a dominant role in this behaviour. Therefore, a question arises: are these results importantly affected by the insufficient vertical resolution of the 1957 samples? To answer it, we present the average relative squared buoyancy frequency variability by water column regions, with values calculated as a function of depth (Table 3) and neutral density (Table 4). Changes in the depth frame include sinking or outcropping of the water masses as well as properties changes along isoneutral surfaces. On the other hand, neutral density representation excludes heaving effects, so only potential temperature and salinity changes along isoneutral surfaces are taken into account.

	CW	**IW**	**UDW**	**MDW**	**LDW**	**BW**
1957 - 1993	0.03 ± 0.06	0.08 ± 0.02	0.03 ± 0.09	0.14 ± 0.08	0.1 ± 0.1	0.2 ± 0.6
1993 - 2010	0.16 ± 0.04	0.06 ± 0.02	0.03 ± 0.02	0.00 ± 0.04	-0.09 ± 0.09	0 ± 1
1957 - 2010	0.15 ± 0.05	0.08 ± 0.02	0.02 ± 0.09	0.14 ± 0.08	0.1 ± 0.1	0.2 ± 0.6

Table 3. Integrated values of the relative variation of squared buoyancy frequency for the depth division of the water column explained in Table 1.

	CW	**IW**	**UDW**	**MDW**	**LDW**	**BW**
1957 - 1993	0.2 ± 0.2	0.2 ± 0.2	0.0 ± 0.1	0.1 ± 0.1	0.0 ± 0.3	0.4 ± 0.6
1993 - 2010	0.2 ± 0.2	0.2 ± 0.2	0.1 ± 0.1	0.05 ± 0.07	0.0 ± 0.2	0.0 ± 0.4
1957 - 2010	0.2 ± 0.3	0.2 ± 0.2	0.0 ± 0.1	0.1 ± 0.1	-0.1 ± 0.4	0.4 ± 0.4

Table 4. Integrated values of the relative variation of squared buoyancy frequency for the different regions of the water column according to the neutral density ranges defined for Table 2.

When using neutral density (γ^n) ranges to divide the water column regions, a generalized rising of the error intervals emerges, what involves higher variability within each γ^n interval. For both representations, even when the mean values adopt positive sign for almost every case, the error intervals often reach negative values, weakening the significance of the information. A positive trend of the variation is observed mainly for central and intermediate waters. Underneath, changes show differences between temporal intervals and both representations. If we consider the higher reliability of the 1993 and 2010 sets of data, due to the better resolution of the original data, we can say that also upper deep waters exhibit a well defined positive trend, as well as a negative trend is observed for lower deep waters. In the same way an enhancement in the case of middle deep waters is obtained for the neutral density representation. Bottom waters variability might be related with to the inability of the 1957 sampling to detect AABW. However, in the case of density representation, changes show an important agreement for the three temporal intervals, what reinforces the validity of the 1957 data for this analysis except for bottom waters. In short, we find a generalised increase of the buoyancy frequency in the whole section throughout the 1957-2010 period, with larger values for central and intermediate waters, the regions showing more intense zonal inhomogeneity.

5. Double diffusive mixing processes: Turner angle.

In the second part of this study, we look at the distributions of the Turner angle to examine the presence of double-diffusive mixing processes along the water column. The distributions illustrated in Figure 8 reveal a similar structure for every realization, controlled by the salty character of the upper-thermocline waters of the North Atlantic. Salt fingering dominates and diffusive convection is almost absent. Diffusive convection only appears in 1993 and 2010 as isolated small-scale patches in the deepest waters of the centre of the basin, as well as somewhere in the western part of the intermediate – deep waters interface.

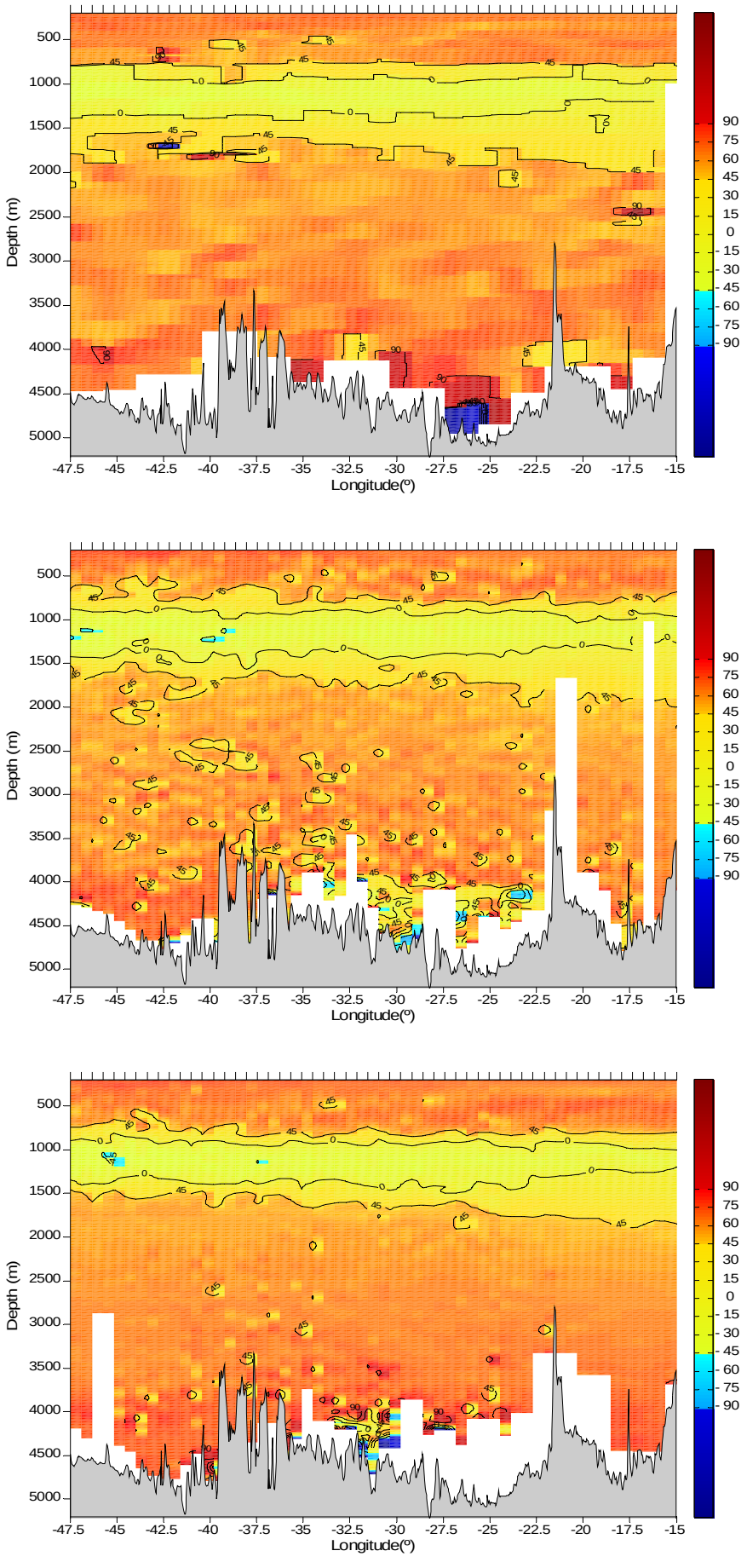

Figure 8. Turner angle (º) distributions for 1957, 1993 and 2010 (upper, mid and lower graph, respectively).

The dominance of salt fingering can be understood once the typical shapes of the potential temperature and salinity profiles are reviewed. Temperature monotonically increases from the end of the mixing layer up to the bottom, providing stability to the water column (generalised positive gradient). On the contrary, salinity exhibits a more complicated behaviour. Below the mixing layer, salinity drops down to approximately 800 m depth to monotonically rise afterwards until depths between 1500 and 2000 m. Underneath, positive gradient extends again up to the bottom. Only a few regions with negative salinity gradients immediately above the bottom escape from this behaviour. In short, those regions in which salinity positive gradients are able to overcome the stabilization effect of the temperature positive gradient, present the potentiality to give rise to salt fingering (Figure 8); albeit turbulence might inhibit the manifestation of these double-diffusive structures. You (2003) obtained a Turner angle atlas, in which the typical shape of *Tu* profile can be deduced, but its zonal distribution is not shown.

The sinking or rising of the profile would cause transitions in the double-diffusive character of the water column. Figure 9 illustrates these Turner angle transitions along the section. The upper panel shows the changes between 1957 and 1993. Transitions from salt fingering to gravitationally stable regimes and the opposite are present (the latter generated by the intense patchiness of the *Tu* in 1993, mid panel of Figure 8). Changes from 1993 to 2010 corroborate that the salt fingering-gravitationally stable transition is dominant in the region of interest and, consequently, rules the whole 1957 to 2010 period (middle and bottom panels of Figure 9). Therefore, the analysis highlights the existence of expanding salt-fingering regions in detriment of the gravitationally stable layer (located ca. between 800 m and 1500-2000 m, depending on longitude). This is caused by a long-term increase of positive salinity gradients, influenced by changes in the intermediate and upper deep waters, respective sources of fresher and saltier water for the equatorial North Atlantic. The larger the entrainment of AAIW (27.4 – 27.8 γ^n range), the wider the vertical extent of the gravitationally stable layer, and the larger the UNADW intrusions in the UDW (27.8 – 27.95 γ^n range), the shallower the gravitationally stable to salt fingering lower interface occurs.

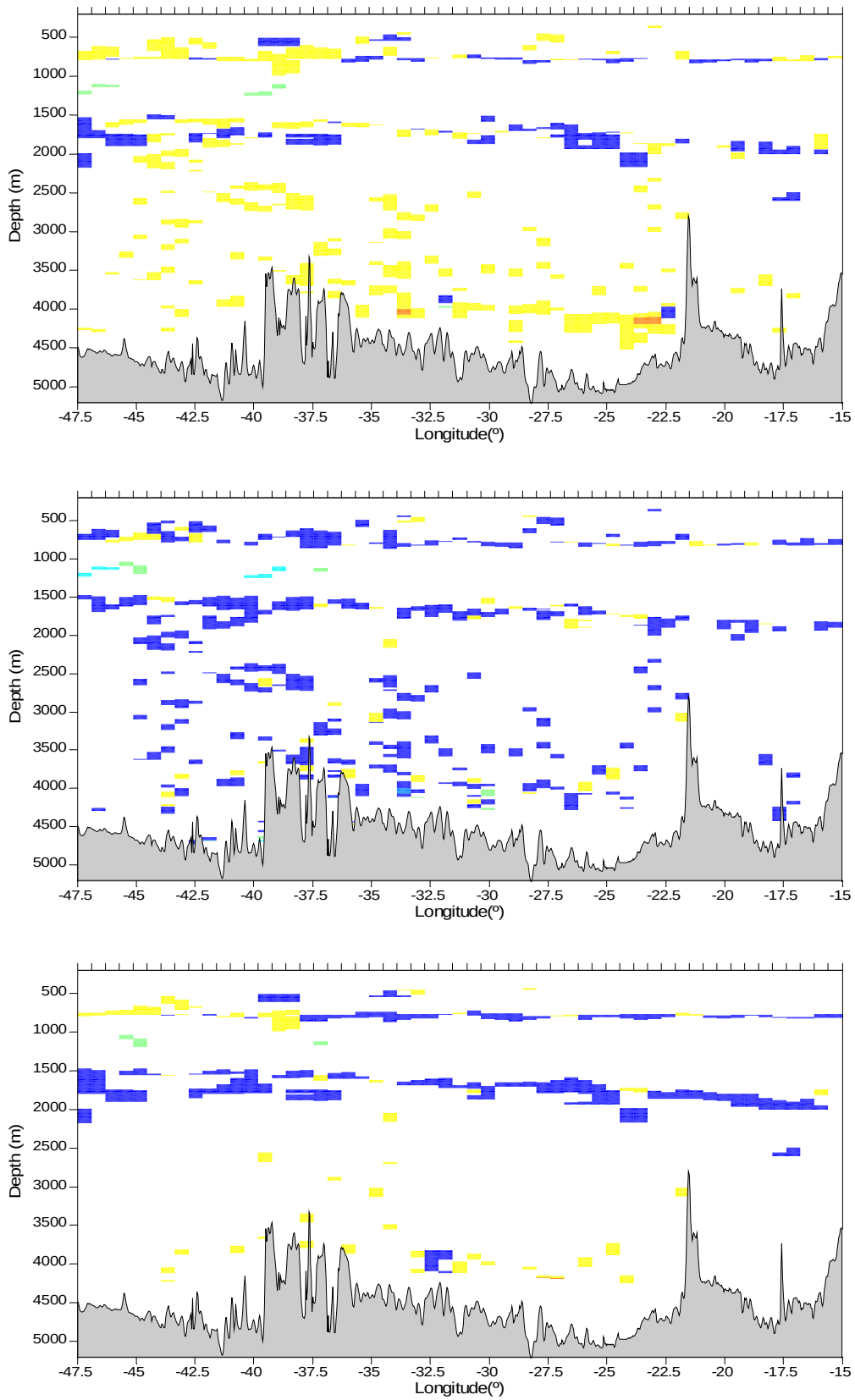

Figure 9. Inter-decadal variation of the mixing double-diffusive character given by the Turner angle (upper, mid and lower graph illustrates the 1957 - 1993, 1993 - 2010 and 1957 - 2010 periods respectively).

The colour code translates as follows: navy blue indicates the transition from gravitational stability to salt fingering; cyan, diffusive convection to salt fingering; turquoise, diffusive convection to gravitationally; green, gravitationally stable to diffusive convection; yellow, salt fingering to gravitationally stable regime and orange, the salt fingering to convective diffusion transformation. (The rest of possible transitions, in white, have not been represented).

Figure 10 depicts the Turner angle distribution according to the already defined γ^n intervals, highlighting a direct relationship between the gravitationally stable *Tu* layer and the intermediate and upper deep waters. Specially clear is the raising of the lower limit of this gravitationally stable layer, which in 1957 lied clearly below the 27.95 isoneutral and in 2010 reaches this value only in the easternmost margin, suggesting an increase in the presence of UNADW. The evolution of the upper limit is nevertheless not so well defined due to the noise of the signal.

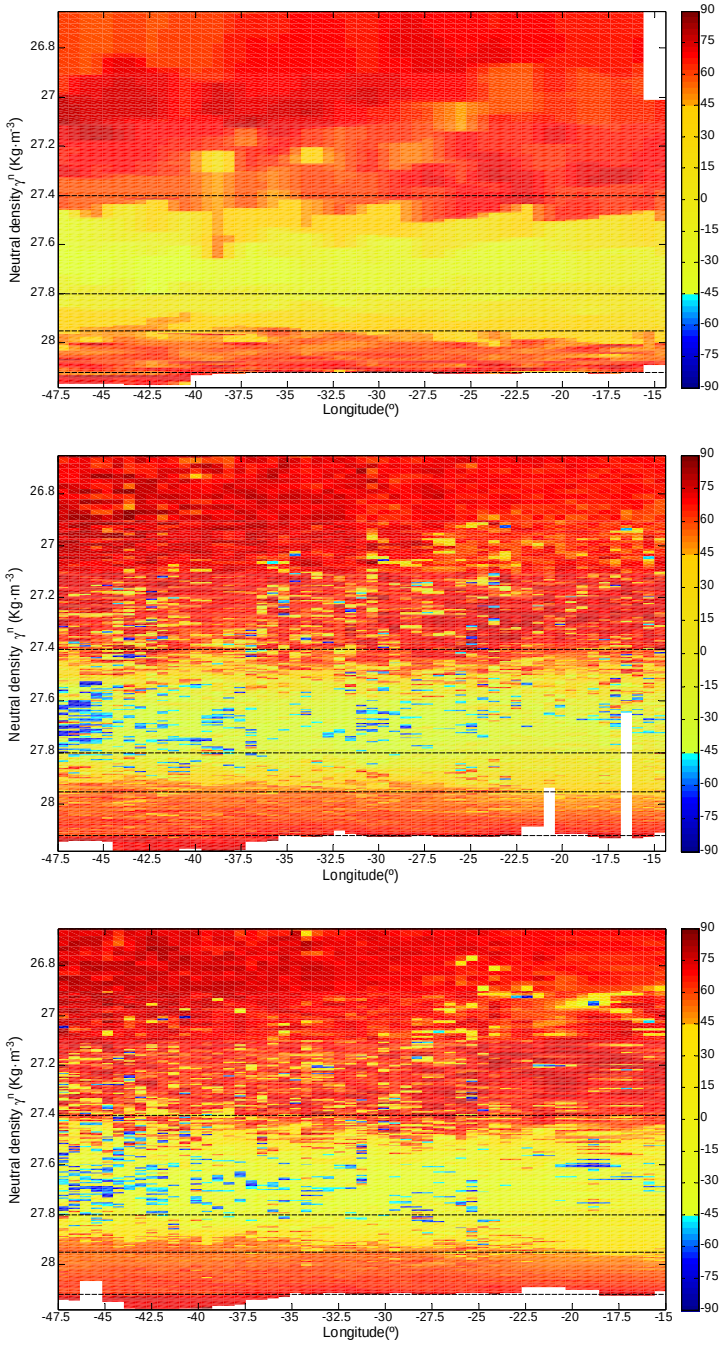

Figure 10. Turner angle distributions for 1957, 1993 and 2010 (upper, mid and lower graph respectively). Interfaces separating central, intermediate, upper deep and bottom waters are shown. Surface waters are not are not included.

To complete the study of the Turner angle variability, the inter-decadal variation of the mixing processes character given by *Tu* is depicted in Figure 11 using neutral density coordinates. This representation confirms the raising of the gravitationally stable lower limit. The deepening of the upper limit is not clarified, so the pattern in Figure 9 for the upper limit may either correspond to the deepening of a given isoneutral or to a temporal decrease in the appearance of AAIW.

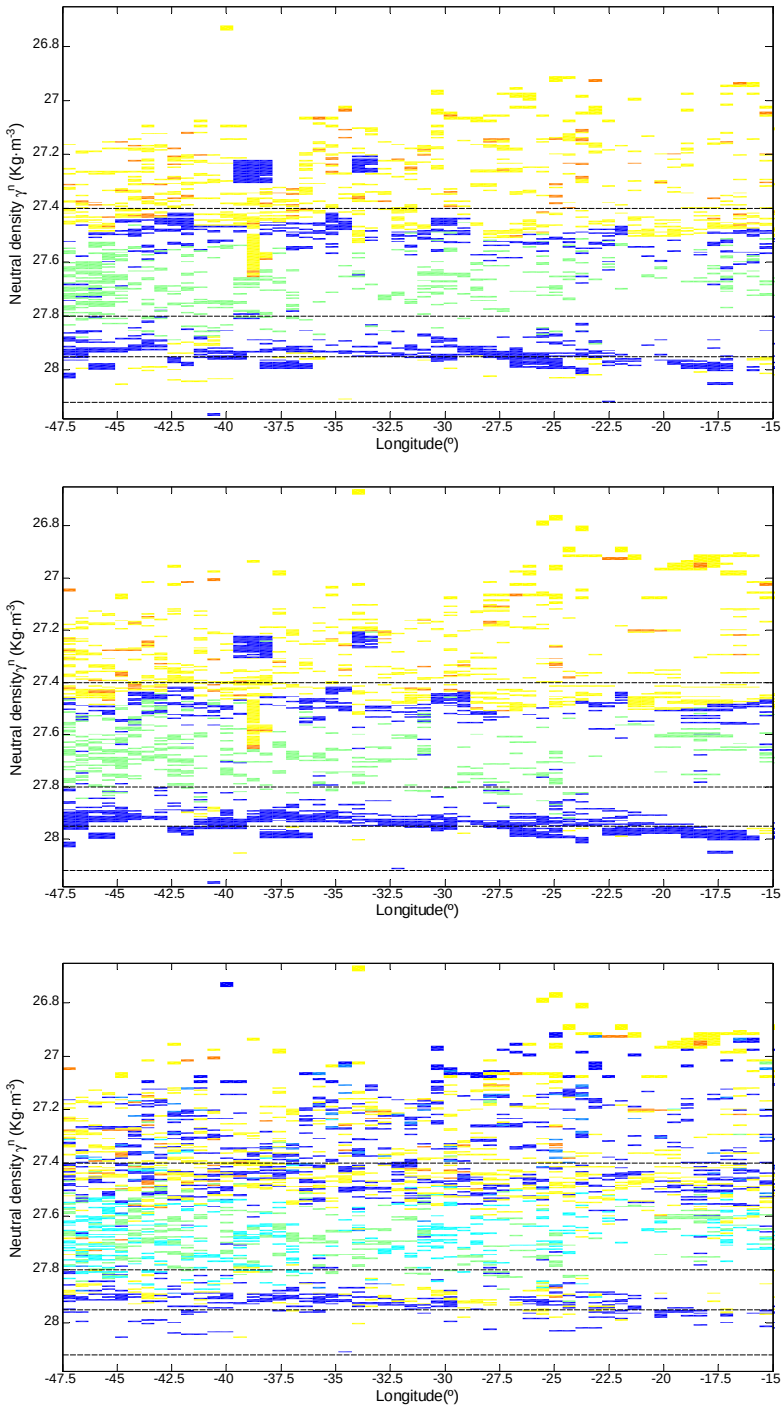

Figure 11. Inter-decadal variation of the double-diffusive character given by *Tu* using neutral density coordinates (upper, mid and lower graph illustrates the 1957 - 1993, 1993 - 2010 and 1957 - 2010 periods respectively).

6. Thermodynamic changes: displacement in the αθ – βS diagrams.

The last studied variable is the dimensionless thermodynamic displacement in the αθ-βS plane. The upper panel of Figure 12 utilizes the 2010 data to reveal the trace of the different water regions in the αθ-βS representation. The most striking observation consists in the appearance of surface, central and upper-intermediate waters along a nearly vertical curve with a constant value of βS about 0.0265. The relatively fresh character of intermediate waters produces the first extreme of the plot, evidenced by a sudden βS increase. Immediately below this water appears the relatively salty UDW, whose presence is revealed by the second extreme in the αθ- βS diagram. Underneath, deep waters follow a nearly constant αθ isoline of about 4×10^{-4} until the appearance of a branching related to bottom waters.

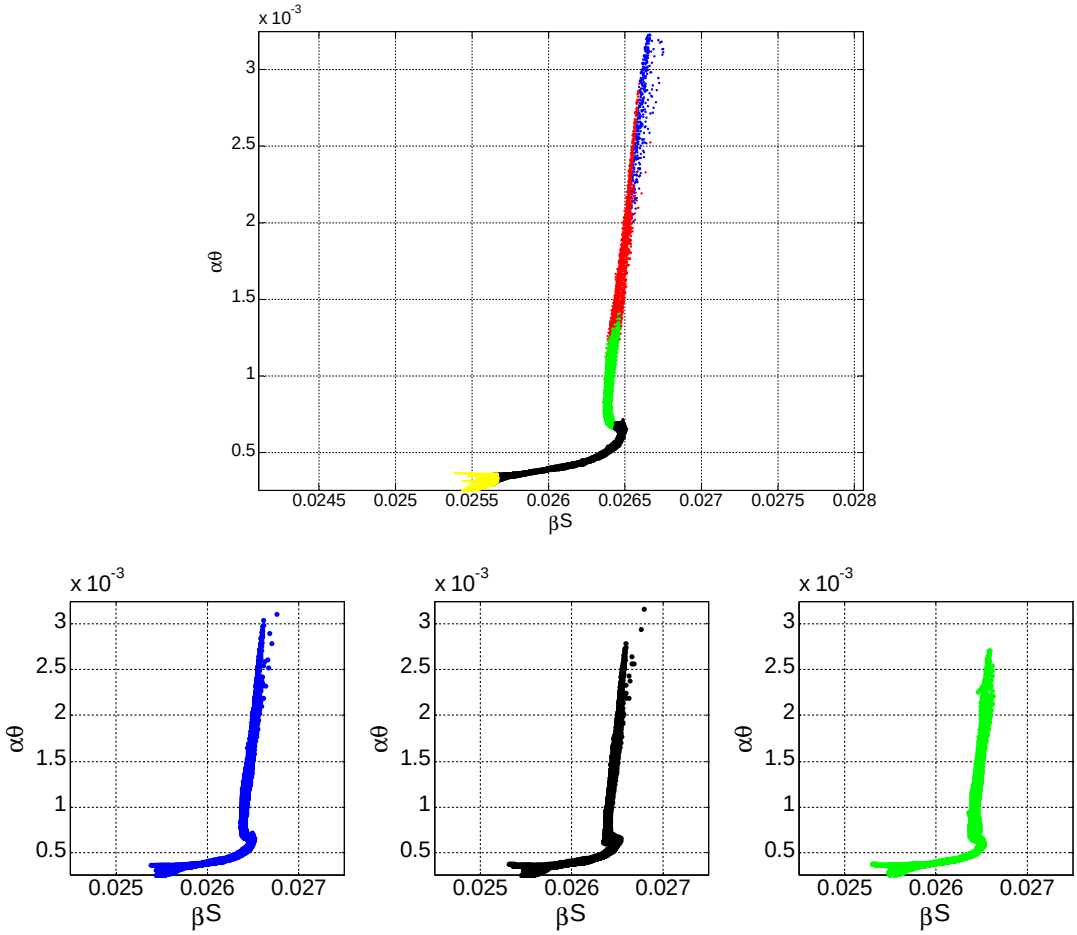

Figure 12. Upper plot: αθ-βS diagram for 2010 transect showing the different depth water regions in different colours. Lower plots: 2010, 1993 and 1957 (from left to right) αθ-βS diagrams (excluding surface waters) for comparison.

The approximate ranges in $\alpha\theta$ are: $> 2\times10^{-3}$ for surface waters, $1\text{-}3\times10^{-3}$ for central waters, $0.6\text{-}1.5\times10^{-3}$ for intermediate waters, $3\text{-}7\times10^{-4}$ for deep waters and $< 4\times10^{-4}$ for bottom waters. These intervals vary between the different repetitions (lower panels in Figure 12) and, of course, depend on the convention used to define the water column regions. βS variations remain insignificant as compared with $\alpha\theta$ for approximately the top 1000 m (surface, central and a large part of intermediate waters). Intermediate and upper deep waters reveal their presence through both extremes, whereas deep and bottom waters behave opposite to the top 1000 m waters since βS variations dominate over $\alpha\theta$ changes.

After having introduced this novel diagrams, our aim is to analyse the thermodynamic displacements as defined by equation (3b). We examine both the spatial distribution of displacements with respect to the mean 2010 profile (spatial displacement) and the temporal changes along the transatlantic section (temporal displacement). An example of the spatial displacement distribution with respect to a mean-transect profile is given in Figure 13. Broadly speaking, the distribution is symmetric both zonally and top-down. Therefore, the highest values of the displacement are located in central (and upper-intermediate) and bottom waters and in both margins (as the reference profile might represent a typical profile of the middle of the basin). Both the eastern and western margins (above all the latter), as well as some central deep waters, display extensive displacements, indicative of significant thermodynamic anomalies with respect to the mean profile.

The inter-decadal displacements are shown in Figure 14. Contrarily to the spatial distribution shown in Figure 13, the inter-decadal *l* maps do not present a general marked top-down symmetry, except in the western region of the basin (ca. between 35 and 47.5 ºW). This is due to the presence of high values related to Antarctic Bottom Water (AABW). Minimum values take place in mid and low deep waters (except west of about 40ºW) and maximum values correspond to central waters. Intermediate and upper deep waters exhibit different behaviour for each time interval. Between

1957 and 1993, the region west of 37.5ºW presents high values up to the sea bottom, whereas values decrease with depth until reaching the UDW for the rest of the section. The 1993 – 2010 pattern is similar but the high values of thermodynamic displacement extend further east for intermediate and upper deep waters, reaching longitudes about 23ºW. The 1957 to 2010 displacement decreases with depth over the whole basin. However, a vertical tongue extending up to approximately 3700 m depth between 45ºW and 41ºW and a shorter one reaching 3000 m depth between 36ºW and 33ºW are present. The largest variations for central and intermediate waters are again confined in the western half. In conclusion, highest values of variation belong to the westernmost zone (west of 35ºW) and to the AABW bed; elsewhere the thermodynamic temporal displacement decreases monotonically with depth.

Table 5 contains the average relative values of the inter-decadal displacements for all water masses. The values remain relatively small (largest values correspond to a 0.6% variation) and monotonically decrease with depth, except for bottom waters. The studied variable is scalar, but the variations in the αθ-βS plane occur in a defined direction, so the 1957 to 2010 displacement corresponds to the vectorial sum of the shorter intervals displacements and not to their direct sum.

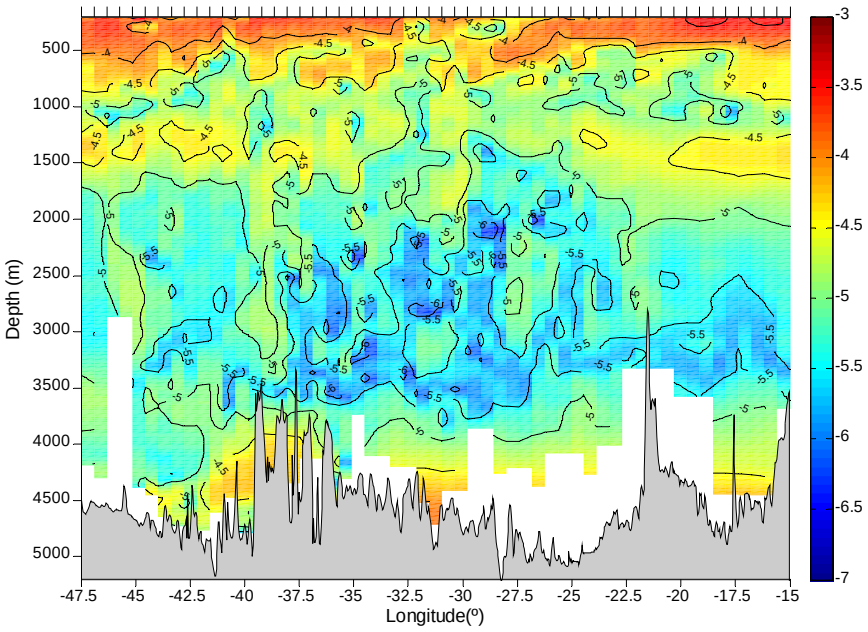

Figure 13. Distribution of the thermodynamic displacement with respect to the mean reference profile for the 2010 transect. Displacements have been filtered by a low-pass Butterworth filter with the aim of smoothing the contours.

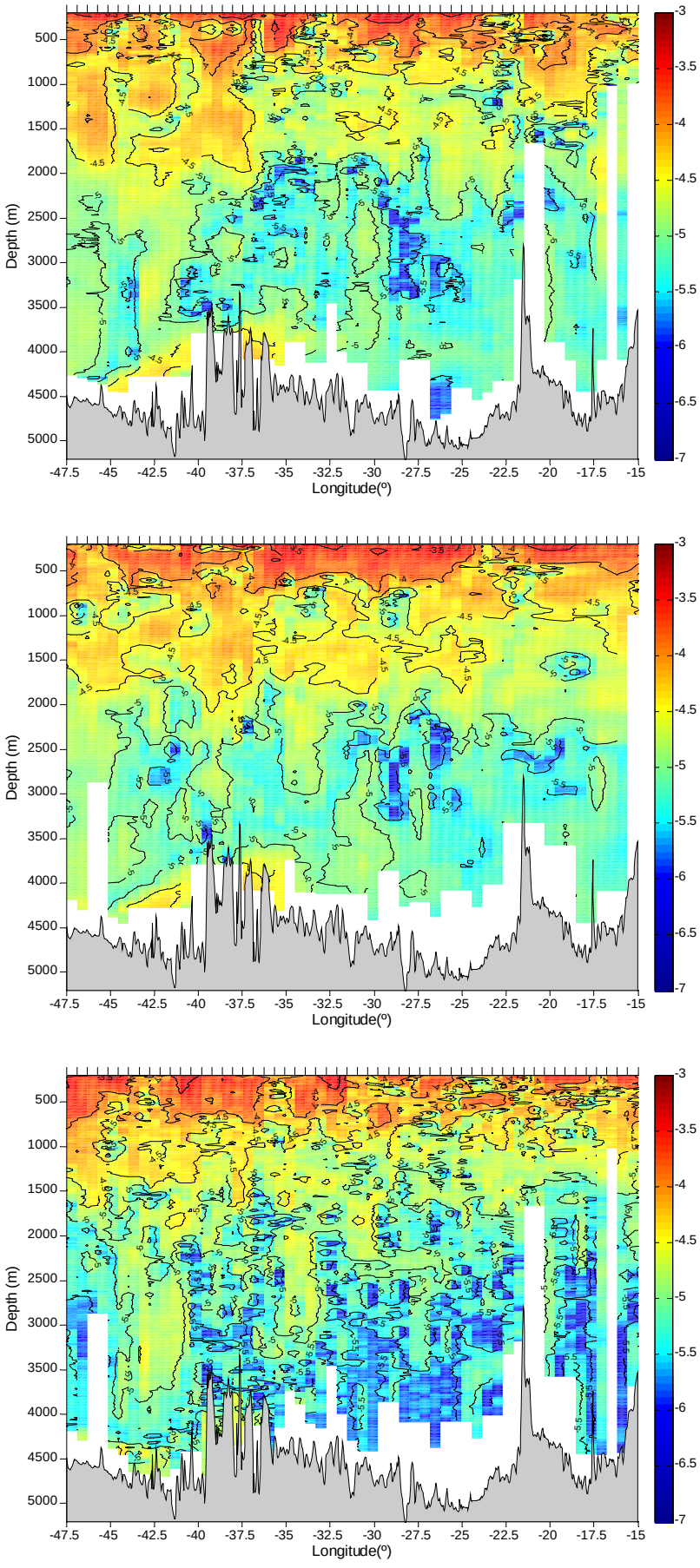

Figure 14. Thermodynamic temporal displacement l (dimensionless, logarithmic map). Upper, middle and lower maps respectively refer to the 1957 – 1993, 1993 – 2010 and 1957 - 2010 variations.

	CW	IW	UDW	MDW	LDW	BW
1993-1957	$(5 \pm 2) \times 10^{-3}$	$(1.9 \pm 0.8) \times 10^{-3}$	$(1.2 \pm 0.1) \times 10^{-3}$	$(4 \pm 2) \times 10^{-4}$	$(3.8 \pm 0.8) \times 10^{-5}$	$(3 \pm 2) \times 10^{-4}$
2010-1993	$(5 \pm 2) \times 10^{-3}$	$(1.9 \pm 0.9) \times 10^{-3}$	$(8 \pm 2) \times 10^{-4}$	$(3.2 \pm 0.8) \times 10^{-4}$	$(2.0 \pm 0.2) \times 10^{-4}$	$(3 \pm 2) \times 10^{-4}$
2010-1957	$(6 \pm 2) \times 10^{-3}$	$(1.9 \pm 0.8) \times 10^{-3}$	$(1.3 \pm 0.2) \times 10^{-3}$	$(4 \pm 3) \times 10^{-4}$	$(4.0 \pm 0.7) \times 10^{-4}$	$(6 \pm 2) \times 10^{-4}$

Table 5. Integrated values of the relative temporal displacement for the different depth regions of the water column.

The distribution of the spatial displacement for the 2010 cruise is presented in Figure 15 as a function of neutral density. The structure of the map reveals important similarities with the analogous maps contained in Figure 13. Central waters adopt the highest values, although contain two tongues of low values lifting eastwards. Intermediate waters present smaller values than the underlying upper-deep waters, which adopt remarkably high values. Below these waters, the displacement decreases again for mid and lower deep waters and even for bottom waters. High values observed for bottom waters in Figure 13 are not observable in this representation.

Figure 16 introduces the inter-decadal displacement *l* analogous to the present in Figure 14, but for γ^n coordinates. This representation expands central and intermediate waters, whereas contracts deep and bottom waters. However, Figure 16 do not highlight relevant deviations from Figure 14, the major difference being a better appreciation of the large values for mid and lower deep waters.

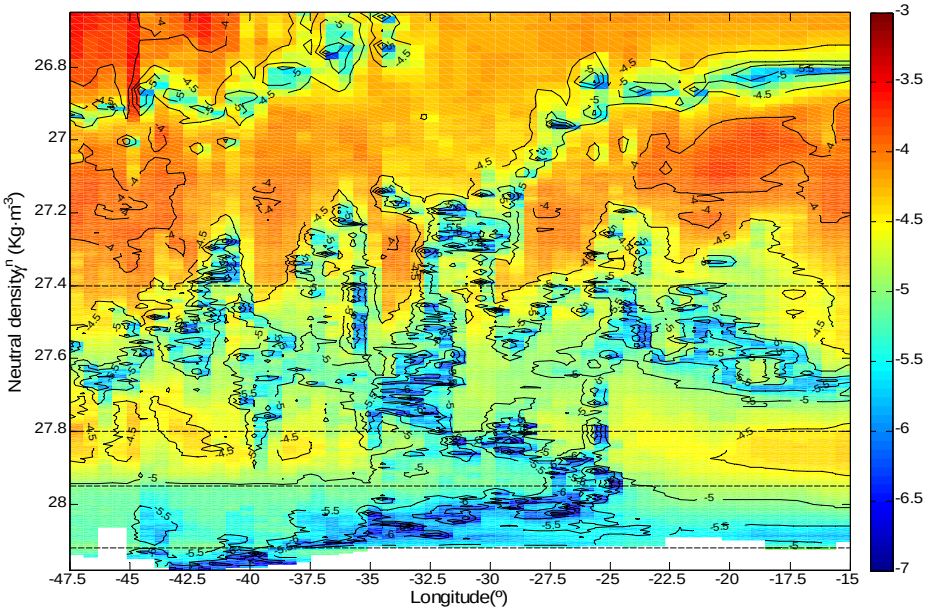

Figure 15. Distribution of the thermodynamic displacement with respect to the mean reference profile for the 2010 transect using γ^n. Surface waters are not are not included in the graph.

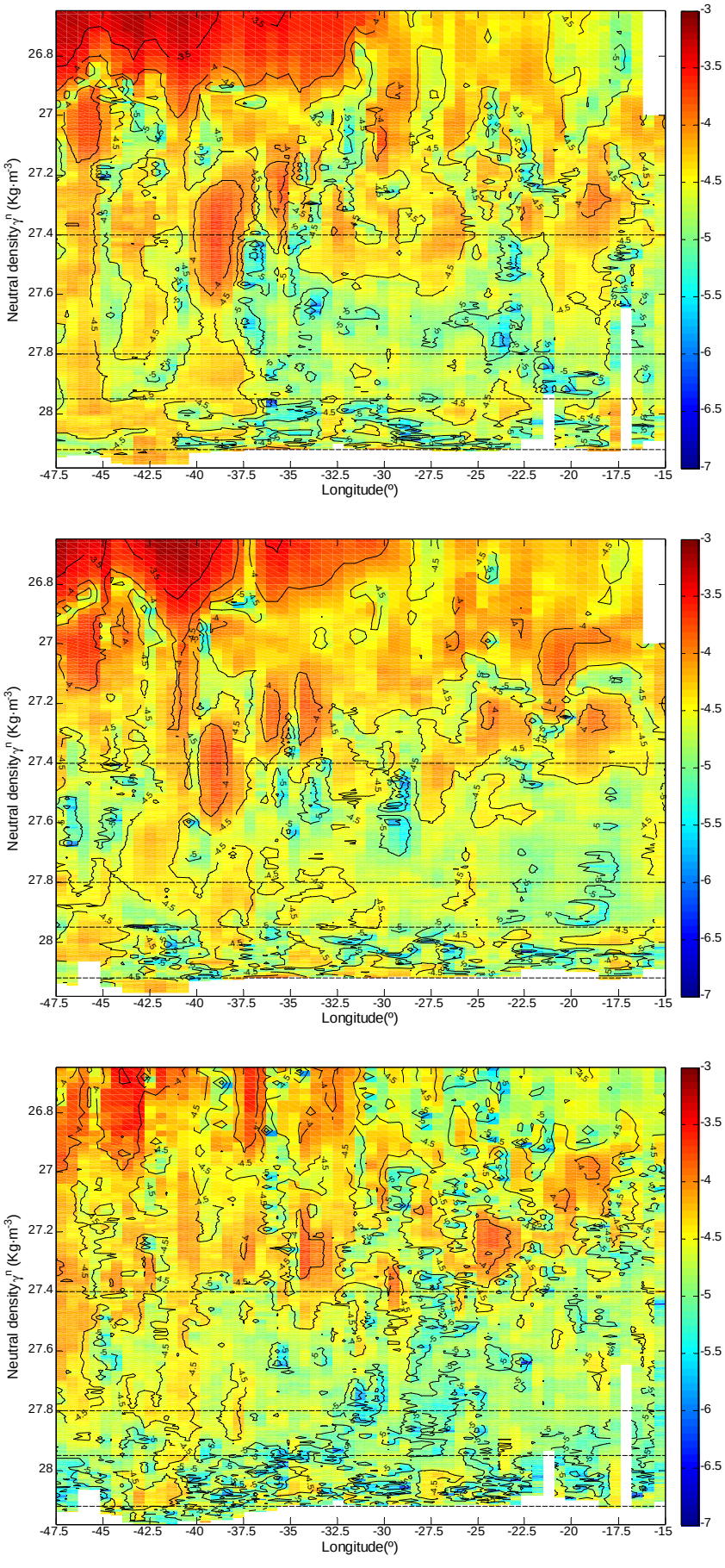

Figure 16. Thermodynamic temporal displacement *l* (dimensionless, logarithmic map). Upper, middle and lower maps respectively refer to the 1957 – 1993, 1993 – 2010 and 1957 - 2010 variations.

Values in Table 6 show important differences with those in Table 5, since they refer to different changes and water regions do not coincide. Within Table 6, similar values are observed for every region and error intervals are small (except for central waters), so changes are well defined.

	CW	IW	UDW	MDW	LDW	BW
1993-1957	$(2 \pm 2) \times 10^{-3}$	$(1.2 \pm 0.4) \times 10^{-3}$	$(9.7 \pm 0.5) \times 10^{-4}$	$(1.1 \pm 0.2) \times 10^{-3}$	$(1.6 \pm 0.4) \times 10^{-3}$	$(2.4 \pm 0.5) \times 10^{-3}$
2010-1993	$(1.8 \pm 0.3) \times 10^{-3}$	$(9 \pm 2) \times 10^{-4}$	$(6.6 \pm 0.8) \times 10^{-4}$	$(7 \pm 1) \times 10^{-4}$	$(8.8 \pm 0.4) \times 10^{-4}$	$(7 \pm 1) \times 10^{-4}$
2010-1957	$(3 \pm 2) \times 10^{-3}$	$(1.1 \pm 0.3) \times 10^{-3}$	$(1.0 \pm 0.1) \times 10^{-3}$	$(1.0 \pm 0.1) \times 10^{-3}$	$(1.4 \pm 0.3) \times 10^{-3}$	$(2.1 \pm 0.3) \times 10^{-3}$

Table 6. Integrated values of the relative temporal displacement for the different γ^n regions of the water column.

7. Conclusions

The distributions of three analysed variables (buoyancy frequency, Turner angle and displacements in the αθ-βS plane) highlight the zonal inhomogeneity of the equatorial Atlantic. Water masses composition and hence water properties drastically change with longitude. The buoyancy frequency distribution presents certain zonal symmetry, excluding the inhomogeneous regions of surface and central waters. Below the latter, buoyancy frequency drops down with depth until reaching bottom waters, which present values even larger than those of low deep waters (not observed in the isoneutral representation). Turner Angle analysis reveals the dominance of salt fingering processes, resulting from the salty character of the North Atlantic. A gravitationally stable layer widening eastwards is observed between around 800 and 1500 – 2000 m, whereas diffusive convection sparsely occurs. Novel αθ-βS diagrams are presented, showing three well-differentiated zones: a linear dependence region for surface, central and upper intermediate waters where αθ changes dominate; a transition zone with two extremes caused by the salinity minimum of AAIW and the salinity relative maximum of UNADW; and finally a nearly horizontal curve within deep waters with the consequent dominance of βS changes.

Thanks to the comparison of the distributions between the three realizations, temporal variations have been identified. Thereby, changes in the potential density profiles between 1993 and 2010 emerge from the Thorpe scale analysis, which reveals an increase in the mean number of potential density overturns per profile and at the same time a reduction of the mean longitude per overturn.

A general increase in the averaged variation of buoyancy frequency is also observed (in spite of the high patchiness and the alternate sign of the variation throughout the section). This positive trend involves increasing static stability, related to more pronounced potential density gradients. Increase reach values around 15% for CW or 8% for IW or 2% for UDW, according to the depth representation, and around 20% for the central and intermediate waters when using neutral density coordinates. Deep and bottom waters manifest different behaviours within each temporal interval, so results seem less consistent than those for central and intermediate waters.

The temporal variation of the Turner angle highlights an increase in salt fingering processes. A slight decrease of AAIW occurs, but this fact is mainly evidenced through the ascension of the lower limit of the gravitationally stable layer caused by the appearance of UNADW in the most recent sections. This observed enhancement of salt fingering processes may intensify the existence of mixing processes. Temporal displacements of the thermodynamic state in the $\alpha\theta$-βS plane generally decrease with depth up to the lower/mid deep waters interface to increase again up to the bottom. Variations stand very small values ($< 0.6\%$), but changes in the two frames (depth and neutral density coordinates) exhibit important differences.

Acknowledgements

This research has been supported by the Spanish government in the frame of project MOC2 (reference CTM2008-06438-C02-01). The author is grateful to the BIO Hespérides scientists, technicians and crew for making possible to gather the 2010 data set.

Thanks to Francis and Josep Lluís for their help, advice, consideration and patience.

References

Arhan, M., H. Mercier, B. Bourles, Y. Gouriou, 1998. Hydrographic sections across the Atlantic at 7º30N and 4º30S. Deep-Sea Research I, 45: 829-872.

Fuglister, F. L., 1960. Atlantic Ocean Atlas of Temperature and Salinity Profiles and Data from the Internacional Geophysical Year of 1957-1958, Atlas Series. Woods Hole Oceanographic Institution, Vol. 1.

Ganachaud, A., 2003. Large-scale mass transports, water mass formation, and diffusivities estimated from World Ocean Circulation Experiment (WOCE) hydrographic data. Journal of Geophysical Research. 108, 3213.

Marin, F., and Y. Gouriou, 2000. Heat fluxes across 7º30'N and 4º30'S in the Atlantic Ocean. Deep-Sea Research I, 47, 2111-2139.

Lappo, S.S., I.D. Lozovatsky, E.G. Morozov, A.V. Sokov, S.M. Shapovalov, 2001. Variability of water structure in the Equatorial Atlantic. Doklady Earth Sciences, 379, 739-743.

Lux, M., H. Mercier, and M. Arhan, 2001. Interhemispheric exchanges of mass and heat in the Atlantic Ocean in January-March 1993. Deep-Sea Research I, 48, 605-638.

Oudot, C., P. Morinb, F. Bauranda, M. Wafar, and P. Le Correb, 1998. Northern and southern water masses in the equatorial Atlantic: distribution of nutrients on the WOCE A6 and A7 lines. Deep-sea Research I 45 (1998) 873-902.

Ruddick, B., 1983. A practical indicator of the stability of the water column to double-diffusive activity. Deep-Sea Research, 30, 1105 – 1107.

Ruddick, B., A.E. Gargett, 2003. Oceanic double-diffusion: introduction. Progress in oceanography , 56, 381 – 393.

Thorpe, S. A., 1977. Turbulence and Mixing in a Scottish Loch. Philosophical Transactions of the Royal Society of London. Series A, Mathematical and Physical Sciences, 286, 125-181.

You, Y., 2003. A global ocean climatological atlas of the Turner angle: implications for double-diffusion and water-mass structure. Deep-Sea Research I, 49: 2075-2093.